OVERVIEW OF RECENT RESULTS FROM THE PHENIX COLLABORATION*

Ron Belmont

University of North Carolina Greensboro, Greensboro, NC 27412, USA

(Received April 11, 2019)

We present recent results from the PHENIX Collaboration on a variety of observables over a wide-range in system size and collision energy.

DOI:10.5506/APhysPolB.50.1003

1. Identified particles

We show a variety of results on nuclear modification factors R_{AA} in large systems with a collision energy of 200 GeV in figure 1. In the left panel, we show the ω meson R_{AA} as a function of p_{T} for Cu+Cu, Cu+Au, and Au+Au

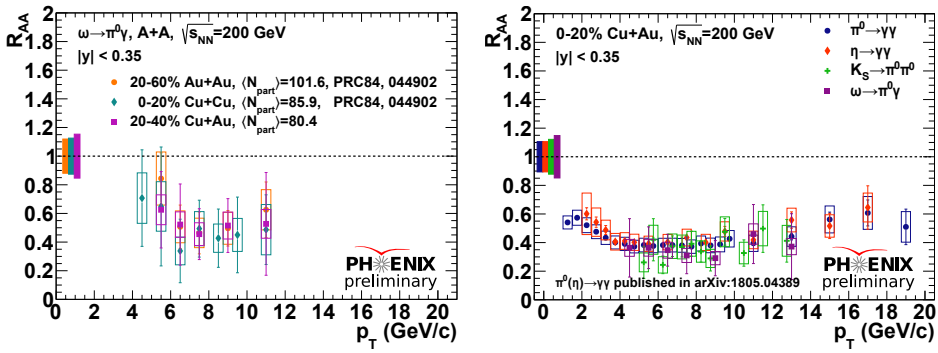

Fig. 1. (Color online) Left panel: R_{AA} of ω mesons as a function of p_{T} in large system collisions at 200 GeV. Indicated by aqua diamonds is Cu+Cu, Cu+Au is shown in magenta square, and Au+Au is represented by orange circles. Right panel: R_{AA} of identified particles in Cu+Au collisions at 200 GeV as a function of p_{T}. Shown in blue circles is the R_{AA} of π^0; red diamonds indicate η mesons; green crosses indicate K^0_{S}; magenta squares indicate ω mesons.

* Presented at the Cracow Epiphany Conference on Advances in Heavy Ion Physics, Kraków, Poland, January 8–11 2019.

in centrality bins selected to approximately match the number of participants $N_{\rm part}$. We see that R_{AA} is essentially completely independent of the collision system when selecting on $N_{\rm part}$, indicating the fairly intuitive result that the overall suppression level is independent of the collision geometry.

In the right panel, we show the $p_{\rm T}$ dependence of R_{AA} of a variety of neutral mesons with different mass and differing strangeness content (π^0, η, $K^0_{\rm S}$, ω) in 0–20% central Cu+Au collisions at 200 GeV. We see a remarkable similarity between each particle at high $p_{\rm T}$, where it seems the hadron mass and strangeness content play little or no role in the observed suppression. Note that this is of course not the case at intermediate $p_{\rm T}$, where strangeness enhancement occurs.

2. Correlations

Figure 2 shows azimuthal correlations of π^0 as the trigger particle with a charged hadron $h^{\pm}$ as the associate particle in Au+Au collisions at 200 GeV. The set of panels in the figure shows the width of the away-side of the correlation function as a function of the associate particle $p_{\rm T}$. The trigger particle $p_{\rm T}$ is indicated in each panel. One sees for lower trigger particle $p_{\rm T}$ values a significant broadening of the away-side correlation function, which appears to be a direct indication of the large-angle radiation expected from gluon bremsstrahlung as partons lose energy traversing the medium. Although not shown, it is worth considering qualitatively the evolution of the double ratio R_I in large systems. This ratio is defined as

$$R_I = \frac{Y^{AA}_{\rm away}/Y^{AA}_{\rm near}}{Y^{pp}_{\rm away}/Y^{pp}_{\rm near}}\,, \tag{1}$$

where Y indicates the yield, and the labels AA, pp, away, and near are all self-explanatory. In p+p collisions, the near- and away-side yields (in a particular angular window) are not necessarily equal due to both the intrinsic

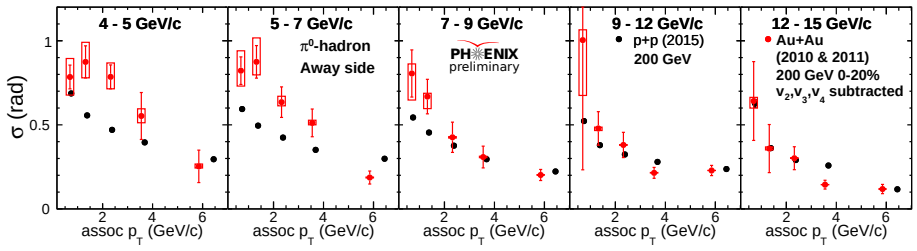

Fig. 2. π^0–$h^{\pm}$ correlations in central Au+Au collisions at 200 GeV. The set of panels shows the width of the away-side of the correlation function as a function of associate particle $p_{\rm T}$. The panels from left to right are in order of increasing trigger particle $p_{\rm T}$; the trigger particle $p_{\rm T}$ range is indicated in each panel.

transverse momentum of the partons in the proton as well as radiative effects in the jets (both of which are referred to as k_{T}). In A+A collisions, additional effects due to the presence of hot nuclear matter can be present. Indeed, for all values of trigger p_{T}, we see an enhancement of associate particles at low p_{T} and a depletion of associate particles at high p_{T}. This appears to be a direct consequence of the momentum shift of the leading parton that fragments into the trigger particle — the depletion at high p_{T} feeds directly into the enhancement at low p_{T}.

Figure 3 shows azimuthal correlations of π^0 as the trigger particle with a charged hadron $h^{\pm}$ as the associate particle in d+Au and ^{3}He+Au collisions at 200 GeV. The left panel shows R_I in d+Au and ^{3}He+Au separately as a function of associate particle p_{T}. Although the effect is small, there is an indication of an enhancement at low p_{T} and a depletion at high p_{T}. The right panel shows the ratio of R_I in d+Au to that in ^{3}He+Au, again as a function of associate particle p_{T}. Although the experimental uncertainties are large, there appears to be a fairly consistent trend that the high-p_{T} depletion in ^{3}He+Au is stronger than that in d+Au. While these results are qualitatively similar to the results in Au+Au, one should exercise extreme caution in interpreting such results. Not only is it possible that these effects could be explained entirely by the presence of cold nuclear matter, but hot nuclear matter suppression may not be expected in small systems anyway. Indeed, as demonstrated in Ref. [1], the apparent suppression in peripheral A+A is likely entirely due to event selection biases and not the physics of particle attenuation. Given the very similar values of N_{part} and N_{coll} between high-multiplicity event categories in small systems and low-multiplicity event categories in large systems, it seems very likely that one should not expect any particle attenuation in small systems. Nevertheless, these measurements provide important constraints on the hard-scattering dynamics in small systems. Active theoretical investigation of these results is encouraged.

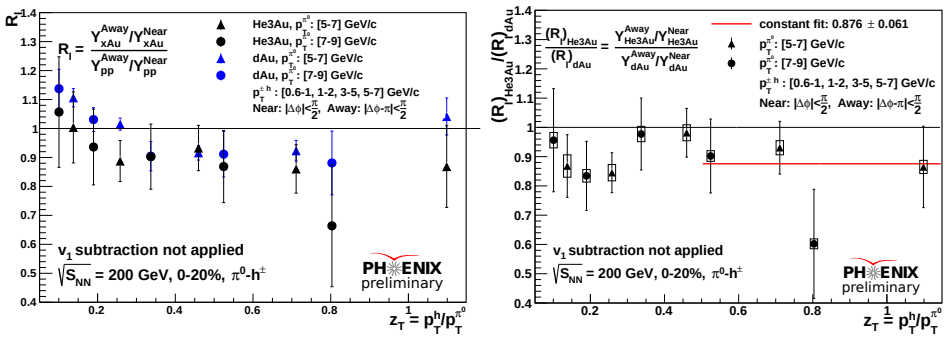

Fig. 3. π^0–$h^{\pm}$ correlations in d+Au and ^{3}He+Au collisions at 200 GeV.

3. Heavy flavor

3.1. Electrons from heavy flavor in large systems

We begin our discussion of heavy flavor by having a look at some recent results on electrons from heavy-flavor decays. Using the central barrel silicon vertex detector, PHENIX has the ability to statistically separate electrons originating from charm quarks ($c \to e$), bottom quarks ($b \to e$), and other sources of non-photonic electrons [2].

We show the p_{T} spectra of electrons from heavy-flavor decays in figure 4. The left panel shows the results in Au+Au collisions at 200 GeV for various centrality bins, and the right panel shows new spectra in p+p collisions [3]. These new p+p spectra will enable a full R_{AA} measurement of flavor separated electrons in various centrality bins.

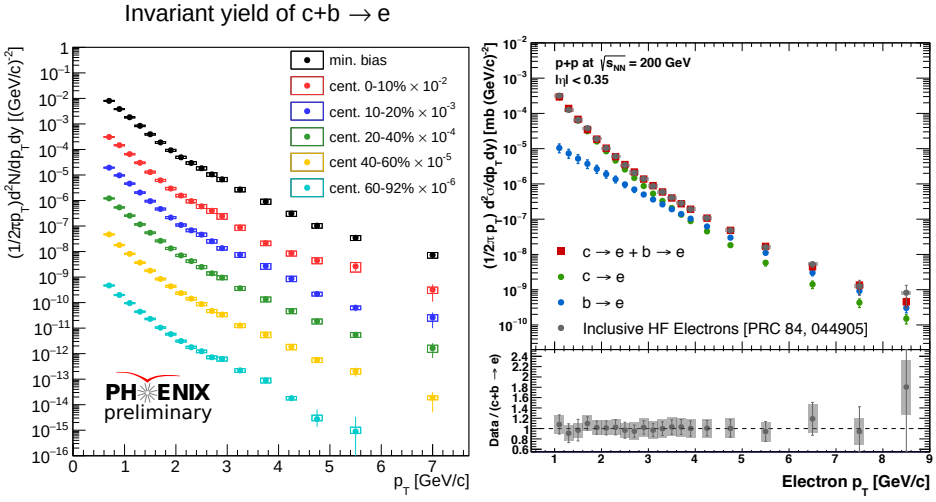

Fig. 4. Invariant yield of heavy flavor electrons as a function of p_{T} in Au+Au collisions (left panel) and p+p collisions (right panel). Right panel figure from Ref. [3].

We show the v_2 of electrons from heavy-flavor decays as a function of electron p_{T} in minimum bias Au+Au collisions at 200 GeV in figure 5. Also shown for comparison is the charged hadron v_2. The left panel shows the electron from charm quark v_2, which is less than the hadron, but is significant and positive. The right panel shows the electron from bottom quark v_2. While the uncertainties are large and the v_2 may be consistent with zero, this is the first measurement of bottom flow at RHIC.

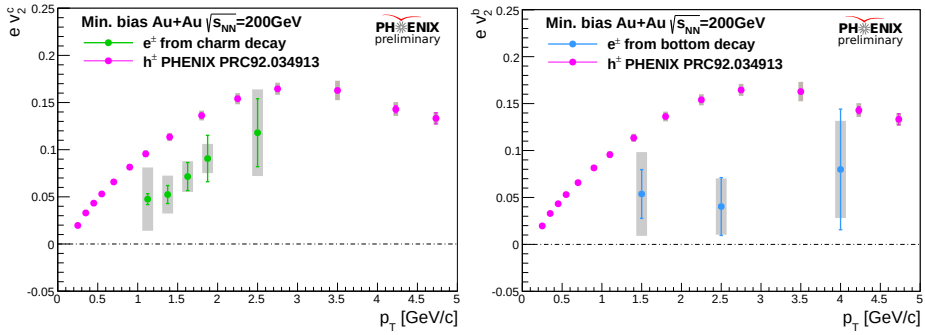

Fig. 5. (Color online) v_2 of electrons from charm (gray/green points, left panel) and bottom (gray/blue points, right panel) decays as a function of electron p_{T} in minimum bias (0–93%) Au+Au collisions at 200 GeV. Shown for comparison in both panels is charged hadron v_2, indicated by the black/magenta points.

3.2. J/ψ nuclear modification factors in small systems

Moving on to small systems, now we will have a look at recent results on nuclear modification factors of J/ψ in a variety of small systems: p+Al, p+Au, and ^{3}He+Au (the d+Au results have previously been published). Figure 6 shows the nuclear modification factors as a function of p_{T} in all three systems for backward rapidity (left panel, $-2.2 < \eta < -1.2$) and forward rapidity (right panel, $1.2 < \eta < 2.2$). The ^{3}He+Au data is very similar to the p+Au data for all p_{T} and in both rapidity ranges. Contrariwise, the p+Al data is quite different. This suggests that the nuclear modification of heavy flavor in small systems depends significantly on the nuclear target but not on the projectile.

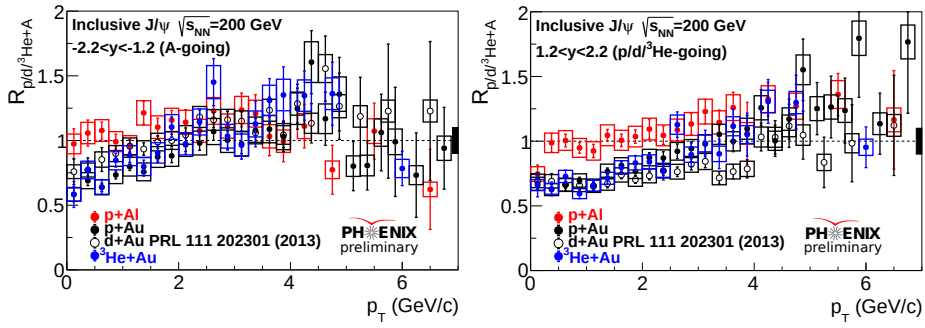

Fig. 6. (Color online) Nuclear modification factors of J/ψ in small systems as a function of p_{T}. The dark gray/red points indicate p+Al collisions; the black points indicate p+Au collisions; the light gray/blue points indicate ^{3}He+Au collisions. All collisions are at 200 GeV.

4. Collectivity in small systems

4.1. Longitudinal dynamics

Figure 7 shows $\mathrm{d}N_{\mathrm{ch}}/\mathrm{d}\eta$ as a function of η in a variety of small collision systems at 200 GeV — p+Al, p+Au, d+Au, and ^{3}He+Au [4]. Also shown are comparisons to the Wounded Quark Model (solid lines) and a 3-D hydrodynamics calculations (dashed lines). Both models describe the mid- and forward-rapidity data very well in all four collision systems. At backward rapidity, the Wounded Quark Model gives a somewhat better description. Also shown in the figure is p+p data from the PHOBOS Collaboration.

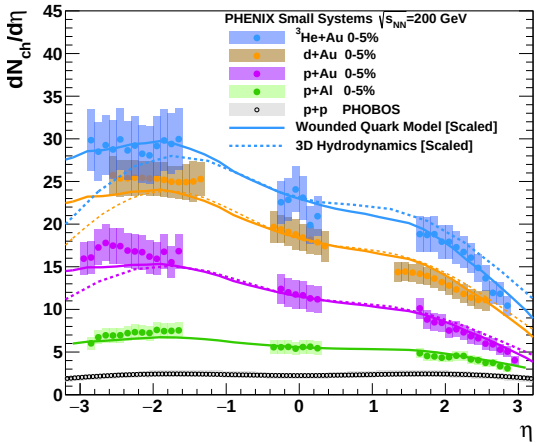

Fig. 7. (Color online) $\mathrm{d}N_{\mathrm{ch}}/\mathrm{d}\eta$ as a function of η in p+Al (first from the bottom/green), p+Au (second from the bottom/magenta), d+Au (third from the bottom/orange), and ^{3}He+Au (fourth from the bottom/blue) collisions at 200 GeV. Shown as solid lines are predictions from the Wounded Quark Model. Shown as dashed lines are predictions from 3-D hydrodynamics. Also shown are p+p data from PHOBOS. Figure from Ref. [4].

Figure 8 shows v_2 as a function of η as light gray/green points in p+Al collisions (far left panel), p+Au collisions (middle left panel), d+Au collisions (middle right panel), and ^{3}He+Au collisions (far right panel) [4]. Shown as solid lines are predictions from 3-D hydrodynamics — there are no calculations yet available for p+Al; the p+Au and d+Au are described very well, while the ^{3}He+Au data are rather different from the calculation. In p+Al and p+Au, prominent peaks at backward rapidity are seen — the event plane detector has a kinematic acceptance of $-3.9 < \eta < 3.1$, so these peaks are easily understood as contributions of short-range correlations. Indeed, this peak is more prominent in p+Al, where the multiplicity is lower and thus there is less combinatoric dilution of the short-range correlations. Furthermore, this contribution becomes clearly subdominant starting

at $\eta \approx -2$, where the expected hydrodynamic trend emerges. The dominance of short-range correlations for $-3 < \eta < -2$ in the p+Au data likely explains the discrepancy with the hydrodynamical calculation in that range. A smaller but qualitatively similar discrepancy exists in the d+Au comparison in the same η range and may have a similar explanation. It is important to remember, however, that flow and non-flow are both vector quantities, meaning they have both a magnitude and a phase. Flow and non-flow need not necessarily have the same phase and, furthermore, the phase difference between them can evolve as a function of kinematic variables.

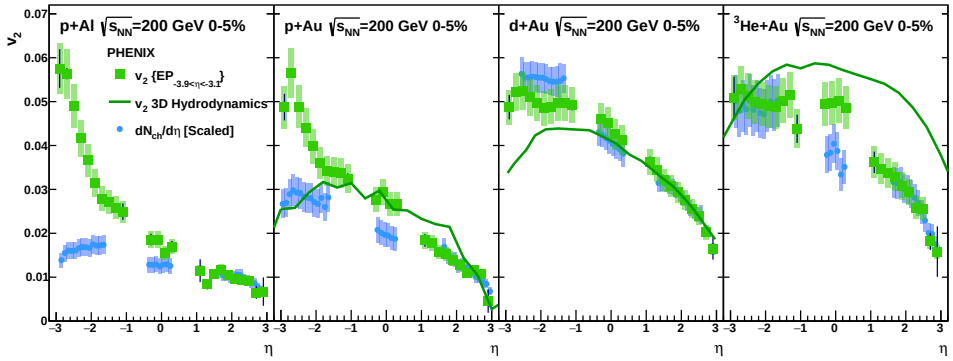

Fig. 8. (Color online) Shown as light gray/green points are v_2 as a function of η in p+Al collisions (far left panel), p+Au collisions (middle left panel), d+Au collisions (middle right panel), and ^{3}He+Au collisions (far right panel). All collision energies are 200 GeV. Also shown as dark gray/blue points are $\mathrm{d}N_{\mathrm{ch}}/\mathrm{d}\eta$ as a function of η, scaled down to match the v_2 at forward-rapidity. Figure from Ref. [4].

Also shown in figure 8 as dark gray/blue points is $\mathrm{d}N_{\mathrm{ch}}/\mathrm{d}\eta$ as a function of η, scaled down to match the forward-rapidity v_2 values. The mid- and forward-rapidity v_2 and $\mathrm{d}N_{\mathrm{ch}}/\mathrm{d}\eta$ have very similar shapes for all four systems; in d+Au and ^{3}He+Au, the backward rapidity also matches reasonably well. The larger systems have higher multiplicity and, therefore, more combinatoric dilution of short-range correlations. However, the apparent absence of short-range correlations may be due to the aforementioned effect of flow and non-flow being out of phase.

4.2. Small systems geometry scan

The small systems geometry scan was undertaken at RHIC to use intrinsic geometry to separate collective effects, which depend on the geometry, from other effects, which are independent of geometry. The three collision species are: p+Au, which has no intrinsic geometry but which can have event-by-event fluctuations into various shapes; d+Au, which has large intrinsic ellipticity (ε_2) due to the shape of the deuteron; and ^{3}He+Au, which

has large intrinsic triangularity (ε_3) due to the shape of the helium-3 nucleus. Qualitatively, one can think of the proton as roughly circular, the deuteron as elliptical, and the helium-3 as triangular, and that the projectile species is the primary contributor to the geometry (see Table I). It is also worth noting that the helium-3 nucleus can have large intrinsic ellipticity, which can be understood by means of a qualitative phasespace picture: the phasespace for the configuration of three nucleons to be a nearly-perfect equilateral triangle is small compared to a configuration where one nucleon is closer (*e.g.* an obtuse isosceles triangle) or further away (*e.g.* an acute isosceles triangle). This can happen both due to the inclination of the helium-3 projectile relative to the target nucleus as well as the nuclear interactions in the nucleus itself.

TABLE I

Ellipticity ε_2 and triangularity ε_3 for p+Au, d+Au, and ^{3}He+Au collisions at 200 GeV. Values from Ref. [5].

System	$\langle\varepsilon_2\rangle$	$\langle\varepsilon_3\rangle$
p+Au	0.24	0.16
d+Au	0.57	0.17
^{3}He+Au	0.48	0.23

Figure 9 shows v_2 (black circles) and v_3 (black diamonds) as a function of p_{T} in p+Au, d+Au, and ^{3}He+Au collisions at 200 GeV [5]. Also shown for comparison are two different hydrodynamical calculations (SONIC and iEBE-VISHNU) and a CGC EFT calculation (MSTV). Both hydrodynami-

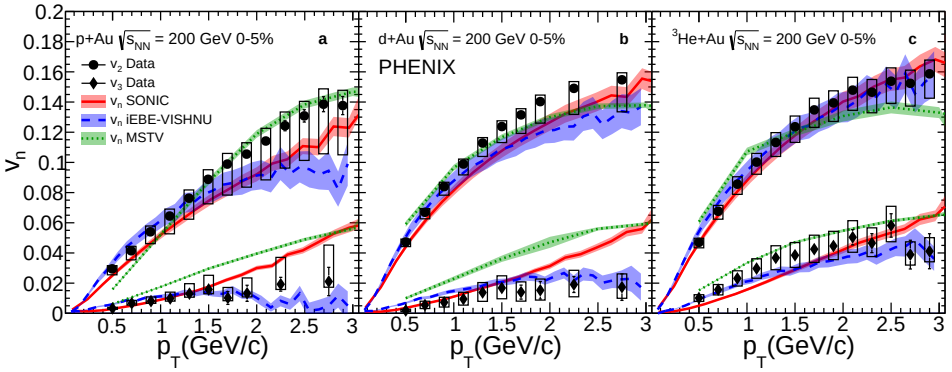

Fig. 9. (Color online) v_2 (black circles) and v_3 (black diamonds) as a function of p_{T} in p+Au (left panel), d+Au (middle panel), and ^{3}He+Au (right panel) collisions at 200 GeV. Also shown are two hydrodynamical calculations (SONIC in solid (red) and iEBE-VISHNU in dashed (blue)) and a CGC EFT calculation (MSTV in dotted (green)). Figure from Ref. [5].

cal calculations describe the data very well. The CGC calculation described the v_2 reasonably well but misses very important features of the v_3. Additionally, the hydrodynamical calculations include hadronization, while the CGC EFT calculation does not — what is shown is gluon v_n as a function of gluon p_{T}. Hadronization will cause a shift in p_{T} as well as considerable angular decorrelation from the parent gluon.

4.3. Electromagnetic probes

Considering the success of hydrodynamics in describing the azimuthal anisotropy in small systems, it is essential to consider additional observables that are highly distinct both in terms of theory behind the physical mechanisms that drive them and the experimental methods that measure them. Electromagnetic probes are ideal for such a consideration. Here, we present the recent PHENIX results on electromagnetic probes in small system.

Shown in figure 10 are the nuclear modification factors R_{pA} of direct photons as a function of p_{T} — the left panel shows minimum bias collisions and the right panel shows central collisions. Seen in both centrality selections is an enhancement of low-p_{T} direct photons. The enhancement is more prominent in central collisions, where the spacetime volume of the system is larger. Also shown in the figure are comparisons to calculations of the expected photon modification in pQCD and hydrodynamics [6]. The data clearly favor the hydrodynamics calculations which include black-body radiation emanating from the spacetime volume.

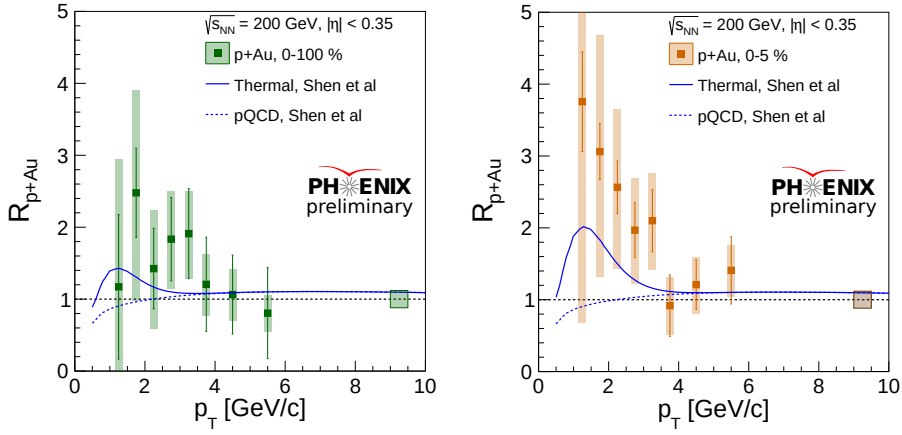

Fig. 10. Nuclear modification factor R_{pA} of direction photons as a function of p_{T} in p+Au collisions at 200 GeV. Minimum bias collisions are shown in the left panel, central collisions (0–5%) are shown in the right panel. Also shown for comparison are calculations of the photon modification in pQCD (dotted lines) and hydrodynamics (solid lines). Theory curves from Ref. [6].

Shown in figure 11 are invariant yields of direct photons for a variety of systems, small and large, at a variety of collision energies. The yields are plotted as a function of the charged hadron multiplicity $\mathrm{d}N_{\mathrm{ch}}/\mathrm{d}\eta$ and fitted to a simple function — it is found that, regardless of centrality and collision energy, the photon yields in large systems (Au+Au and Pb+Pb) are directly proportional to $(\mathrm{d}N_{\mathrm{ch}}/\mathrm{d}\eta)^{\alpha}$, where α is empirically determined to be 1.25 [7]. If one takes data from p+p collisions and applies the same empirical scaling, one sees a large gap between p+p and large systems. This is straightforwardly understood as enhancement due to thermal emission of photons. What is remarkable, however, is the observation that the small systems p+Au and d+Au fit nicely in between these two trends, suggesting a turn-on of thermal radiation.

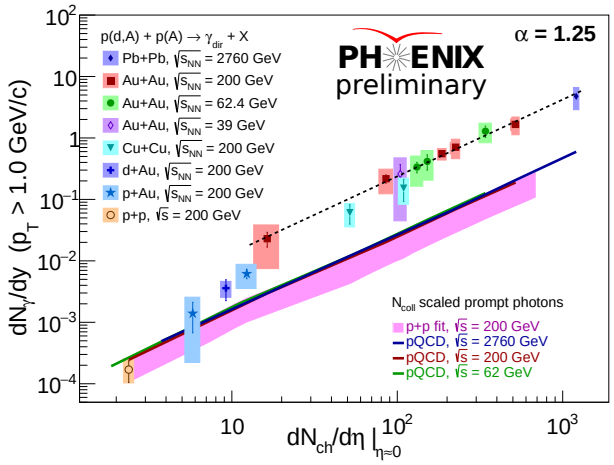

Fig. 11. Invariant yield of direct photons as a function of charged hadron multiplicity $\mathrm{d}N_{\mathrm{ch}}/\mathrm{d}\eta$.

REFERENCES

[1] C. Loizides, A. Morsch, *Phys. Lett.* **B773**, 408 (2017).
[2] A. Adare *et al.*, *Phys. Rev.* **C93**, 034904 (2016).
[3] C. Aidala *et al.*, `arXiv:1901.08405 [hep-ex]`.
[4] A. Adare *et al.*, *Phys. Rev. Lett.* **121**, 222301 (2018).
[5] C. Aidala *et al.*, *Nature Phys.* **15**, 214 (2019).
[6] C. Shen *et al.*, *Phys. Rev. C* **95**, 014906 (2017).
[7] A. Adare *et al.*, `arXiv:1805.04084 [hep-ex]`.